Foam improved oil recovery: Foam front displacement in the presence of slumping

Elizabeth Mas-Hernández, Paul Grassia*, Nima Shokri

CEAS, The Mill, The University of Manchester, Oxford Road, Manchester M13 9PL, UK

Abstract

Foam is often used in improved oil recovery processes to displace oil from an underground reservoir. During the process, the reservoir is flooded with surfactant, and then gas is injected to produce foam in situ, with the foam front advancing through the reservoir. Here the effect of surfactant slumping (downward movement of surfactant in relation to a lighter phase) upon the advance of a foam front is presented. Slumping which can be associated with foam drainage, coarsening and collapse, causes a rise in mobility of the foam front specifically near the top of the front. The description of a foam front displacement for an initially homogeneous foam mobility is therefore modified to account for slumping-induced inhomogeneities. Numerical solution for the front shape shows that, although slumping transiently produces a localised concave region on the otherwise convex front, this concavity has little effect on the long term front evolution. In fact in the long-time limit, a *convex* kink develops on the front: an analytical solution describing the convex kink agrees very well with the numerics.

Keywords: Improved-oil recovery, Foam, Pressure-driven growth, Porous media, Numerical solution, Analytical solution

1. Introduction

Surfactant and gas are often injected into underground oil reservoirs so as to produce foam that can subsequently displace oil and achieve improved oil recovery: under these circumstances engineers wish to predict how the foam front advances through the reservoir displacing the oil. In the calculations of foam front movement through an oil reservoir an idealized model for so called surfactant-alternating-gas (SAG) injection [1, 2], is used. The model is known as 'pressure-driven growth' [3].

In what follows we introduce the 'pressure-driven growth' model with a minimum of detail as it is already well discussed in literature [1, 2, 3]. However the appendix provides additional detail about the model for readers who require it.

During the surfactant-alternating-gas (SAG) process a foam bank advances into an oil reservoir that has already been flooded with surfactant in aqueous solution (the so called liquid bank). The pressure driving the foam is the difference between the injection pressure and the hydrostatic pressure (the latter of course varying with depth). The pressure-driven growth model assumes (with some justification from so called fractional flow theory [1]) that most of the resistance to the foam motion

*Corresponding author

Email address: paul.grassia@manchester.ac.uk (Paul Grassia)

arises from a region of wet foam located right at the foam front, and moreover this resistance grows according to the distance that the front has displaced (because the wet foam region gradually thickens over time). Balancing the driving pressure force with the resistance leads to a prediction for the speed of material points on the foam front, the direction of motion being normal to the front.

Mathematically the model consists of a system of differential equations for the motion of the material points, the equations being solved numerically [2], in our case with an algorithm programmed in Matlab.

The system of equations can be conveniently written in dimensionless form, using scales identified by [1] (see also the appendix). The dimensionless equations describing the system (1)–(3) are shown below:

$$\frac{\mathrm{d}X_D}{\mathrm{d}t_D} = \frac{(1 - Z_D)\cos\alpha}{s_D} \tag{1}$$

$$\frac{\mathrm{d}Z_D}{\mathrm{d}t_D} = \frac{(1 - Z_D)\sin\alpha}{s_D} \tag{2}$$

$$\frac{\mathrm{d}s_D}{\mathrm{d}t_D} = \sqrt{\left(\frac{\mathrm{d}X_D}{\mathrm{d}t_D}\right)^2 + \left(\frac{\mathrm{d}Z_D}{\mathrm{d}t_D}\right)^2} \tag{3}$$

where X_D gives horizontal position in a rectangular reservoir, Z_D the vertical position (measured downwards from the top), t_D is the time, s_D the distance the front travels, and α the angle giving the front orientation as depicted in Figure 1 (specifically $\tan\alpha = -\mathrm{d}Z_D/\mathrm{d}X_D$, implying that equations (1)–(3) are partial differential equations in space and time, rather than ordinary differential equations in time only). Note that $Z_D = 1$ corresponds to the point at which hydrostatic pressure balances injection pressure: the front cannot advance to depths beyond $Z_D = 1$.

The initial and boundary conditions are:

$$X_D(Z_D, 0) = 0 \tag{4}$$

$$s_D(Z_D, 0) = 0 \tag{5}$$

$$\alpha(0, t_D) = 0. \tag{6}$$

In the implementation of the initial conditions in the computer program, those given by equations (4) and (5) are changed to $X_D(Z_D, 0) = s_D(Z_D, 0) = s_{D_0}$ where s_{D_0} is a small parameter (typically chosen here to be $s_{D_0} = 0.001$) to avoid having infinite values of $\mathrm{d}X_D/\mathrm{d}t_D$ and $\mathrm{d}Z_D/\mathrm{d}t_D$ at $t_D = 0$. Starting from a vertical front, for a homogeneous medium (i.e. a homogeneous reservoir, with in addition, foam mobility being homogeneous along the front), the system tends to give a convex shape for the front at finite time: the top of the front advances more than parts lower down because the difference between injection pressure and hydrostatic pressure is greater at the top.

Boundary condition (6), which according to the definition of angle α says that material instantaneously at the top of the reservoir is moving parallel to the top, implies also that the top of the front has unit speed at the particular time when it has displaced by unit distance. The volume swept by the front grows over time, albeit this rate of sweeping volume slows down as time proceeds.

Numerical solution for pressure-driven growth, i.e. discretising the front shape

and computing the evolution of the discretised front material points, is known to present challenges [2, 3]. In our numerical implementation it is possible to trace the front displacement until large times, and still have a fair representation of its shape, because a rule has been implemented for subdividing front segments whenever they become too long, which occurs particularly near the top of the reservoir. Such a rule is given by equation (7); where the subscript 0 indicates a point at the top of the reservoir, the subscript 1 refers to the next point below the top, and n indicates a new point between these two.

$$X_{D_n} = X_{D_0} - \left(\frac{Z_{D_0} - Z_{D_n}}{Z_{D_0} - Z_{D_1}} \right)^{3/2} (X_{D_0} - X_{D_1}) \,. \tag{7}$$

This equation respects a known mild singularity [3] for the front curvature at the top boundary: specifically it has been shown [3] that in the limit of very small Z_D values, the amount that X_D falls behind the leading edge at the top of the reservoir is proportional to $Z_D^{3/2}$, corresponding to a curvature scaling proportional to $Z_D^{-1/2}$. Further details about this singularity and why it arises are given in the appendix.

As already mentioned above, the foam front (at least for a homogeneous system) is expected to have a convex shape. This is somewhat fortunate, because concavities are known to be extremely problematic when implementing pressure-driven growth [3]. Nevertheless, even small concavities in the shape of the curve caused by numerical artifacts (for example, truncation and/or round-off error accumulation) or by the physical nature of the system (e.g. if the medium is not perfectly homogeneous) could lead to a completely distorted shape of the curve, as concave points tend to fall increasingly far behind their neighbours [3].

The evolution of concavities over time, if they are not addressed, causes the formation of spurious loops [3] (regions where points of the front cross over each other). Spurious loops are generated whenever the points towards the back of a concavity are left behind but the points further ahead converge towards each other and cross over one another. Points towards the back of a concavity can have their velocities corrected to avoid them falling behind (the corrected version represents the physics that we want the pressure-driven growth model to capture [3], specifically the backs of the concavities constitute 'shocks' which have a different speed from front material points which constitute 'characteristics' of the governing partial differential equations). The velocity correction does however cause the length of the intervals towards the back of the concavity to decrease over time, in turn requiring implementation of a rule to eliminate short intervals. For these reasons, it is necessary that the algorithm be able to deal with both concavities and shrinking intervals.

Our way to handle the presence of concavities in the front shape is, as mentioned above, by applying a correction in the velocity calculations (the correction being reflected in the time derivatives, equations (1) and (2) in the original system) when certain criteria on the degree of concavity are met. This aims to speed up the displacement of points in the concave regions to catch up with those in the convex region and in this way return towards a convex shape for the entire foam front (or, at the very least, to keep the concavity localised and contained). The corrected velocities are [3]

$$\frac{\mathrm{d}X_D}{\mathrm{d}t_D} = \frac{(1 - Z_D)\cos\alpha}{s_D \cos\frac{\theta}{2}} \tag{8}$$

$$\frac{\mathrm{d}Z_D}{\mathrm{d}t_D} = \frac{(1 - Z_D)\sin\alpha}{s_D \cos\frac{\theta}{2}} \tag{9}$$

where X_D, Z_D, α, t_D, and s_D are defined previously, and θ is the angle through which the tangent turns between the midpoint of the segments and is given by equation (10),

$$\theta = \arccos(\mathbf{t_2} \cdot \mathbf{t_1}) \tag{10}$$

where $\mathbf{t_1}$ and $\mathbf{t_2}$ are the tangents of adjacent segments on the curve (or strictly speaking on the discretised representation thereof): see Figure 2.

In the computer program, an 'if' construction is used to decide when to use the alternate formulae with a criterion considering both a negative curvature (the way curvature, K, is defined establishes it as negative for concave regions and positive for convex regions) and the magnitude of the turning angle (θ). Curvature is described in equation (11):

$$K = \frac{(\mathbf{t_2} - \mathbf{t_1})}{\frac{1}{2}d_2 + \frac{1}{2}d_1} \cdot -\mathbf{n} \tag{11}$$

where $\mathbf{t_1}$ and $\mathbf{t_2}$ are the tangents of adjacent segments on the curve, d_1 and d_2 the length of those segments, $\mathbf{n}$ the normal vector in direction of the front movement: again see Figure 2.

Meanwhile a small finite angle (θ_{sharp}, the sharpest turning angle we permit) is set and compared to θ. A previous study gave consideration to how values of θ_{sharp} might be chosen, suggesting that any choice of θ_{sharp} significantly less than unity (but larger than the dimensionless length of discretised elements on the front) would have the desired effect of keeping concavities localised and contained, and moving them in a way that was compatible with the surrounding convex parts of the front. The criteria for the 'if' statement become as follows: if $K < 0$ and $\theta > \theta_{sharp}$, then we use equations (8)–(9) in lieu of equations (1)–(2). We assumed $\theta_{sharp} = \pi/18$ here. The above formulae and criteria are implemented in a new version of the 'pressure-driven growth' program that is able to deal with concavities (i.e. keep them localised and contained) and evolve back towards a predominately convex shape for the displacement front.

As mentioned above, there are cases, not solely arising from numerical error, but rather from the physics of the problem itself, where concavities are present. Such cases include [3] a heterogeneous reservoir (as alluded to above), increase of the injection pressure, and also so called liquid/surfactant slumping. The following sections deal with the case of liquid/surfactant slumping and the two other cases will be addressed in future work.

The remainder of this paper is laid out as follows. The physics of slumping is discussed in section 2, and a mathematical model for slumping within the context of pressure-driven growth is presented in section 3. Results are given in section 4, and these are used as the basis to derive a long-time asymptotic description of the front shape resulting during the slumping process in section 5. Conclusions are offered in section 6.

2. Slumping

In the process of interest here, injection of foam in an oil reservoir, slumping (i.e. downward migration of a heavier phase relative to a lighter one) can refer to liquid or surfactant; in both cases it takes place due to downward flow (whether of liquid

relative to gas, or surfactant solution relative to surfactant-free liquid) but can have slightly different effects on the foam front itself, which are described in more detail below (along with the root causes). However, before stating the subtle difference between these two phenomena, it is important to explain why such processes affect foam front displacement at all.

The displacement of the foam front over time is affected by drainage and coarsening/collapse of the bubbles that make up the front. The effect these processes have on the bubble size is what ultimately leads to the increase of mobility in the topmost region of the reservoir. It is important to note that the description of drainage and coarsening/collapse here is not sophisticated: it is used mainly to explain the increase in mobility, an increase which we will represent empirically. It is this mobility increase which then affects the front displacement. There are different factors that contribute to this mobility increase which are explained below.

The liquid in the films tends to move downwards due to the effect of drainage driven by gravity, because it is heavier than gas [4, 5, 6]. On the other hand, the gas inside the bubbles tends to migrate upwards. As a consequence, the bubbles at the top become drier and as time passes they collapse [4, 6, 7], leaving behind a foam with coarser bubbles. Meanwhile surfactant solution moving downwards relative to surfactant-free liquid makes the foam films less stable (i.e. more liable to collapse) at the top, again producing coarser bubbles. Again the downwards migration of surfactant solution is gravity-driven, based on the density difference with surfactant-free liquid, even though the actual density difference involved will be far less than that between liquid and gas. Thus both liquid and surfactant slumping will be the cause of foam collapse. However the mechanisms are different: liquid slumping affects stability by making foam become drier at the top, whilst surfactant slumping will make foam less stable (even if the liquid fraction is unchanged) [3].

Previous work, including experiments and simulations [7, 8, 9, 10], show that vertical arrangements of foams have bigger and drier bubbles at the top and, smaller and wetter bubbles at the bottom. These experiments were performed for two-dimensional foams of various levels of polydispersity; despite this, the results are loosely comparable to our case of a thin foam front in porous media. In summary, the phenomena of drainage and coarsening/collapse affect the texture of foams (i.e. bubble diameter and distribution of small and big bubbles within the foam). This texture however then influences mobility.

For foam flow through porous media, fewer films implies less dissipation. Bigger and drier bubbles at the top result in an increase of the mobility [11, 12]. For the model used here (pressure-driven growth), the mobility at the front itself is considered low compared to the water bank ahead and the gas bank behind the front where mobility has a much greater value [1]. However, owing to slumping, the mobility in the region of the top part of the front will be slightly larger than the front mobility lower down.

As a consequence of the increase in mobility in the top region of the reservoir, which only should happen once slumping onsets after finite time, the shape of the curve representing the foam front need not remain convex. It was postulated [3] that instead concave regions can start to develop as shown schematically in Figure 3, due to material on the front higher up starting to move substantially faster than material lower down.

In actual fact, liquid slumping is expected to occur *after* the contact between the liquid and gas phases, which is when the foam front has already passed a given

point in the reservoir. This is merely saying that liquid only drains from foam once the foam itself is formed. Accordingly, liquid slumping strictly speaking needs to take into account the change in mobility behind the foam front [3]. Therefore, the model studied here, pressure-driven growth, is not suitable in this case because it focuses on the mobility of the foam front itself. Since the mobility of the foam bank away from the foam front is already assumed in our model to be exceedingly high compared to that of the front itself, a further increase in foam bank mobility due to slumping does not impact on the model.

Surfactant slumping, on the other hand, can take place before the front arrives at some specified point of the reservoir (and so, when the front subsequently arrives at that point, affects the texture of the foam as it is being produced right at the front). The foam front mobilities *are* included in our pressure-driven growth model and surfactant slumping affects them. Hence pressure-driven growth seems more convenient for modelling surfactant slumping, so that is the situation we envisage here.

For the description of slumping at the front, the velocity formulae for material points need to reflect the above mentioned feature (the increase of mobility at certain vertical positions near the top of the front). The next section presents the pertinent equations for the slumping case and explains the approach to solve them numerically.

3. Model for slumping

To model the effects of slumping on the front, the system can be defined by equations (12) and (13) for the horizontal and vertical components of the velocity

$$\frac{\mathrm{d}X_D}{\mathrm{d}t_D} = \frac{M_{slump}(1 - Z_D)\cos\alpha}{s_D} \tag{12}$$

$$\frac{\mathrm{d}Z_D}{\mathrm{d}t_D} = \frac{M_{slump}(1 - Z_D)\sin\alpha}{s_D} \tag{13}$$

where X_D, Z_D, s_D, t_D, and α are defined previously; and M_{slump} is the relative increase in mobility (compared to the case with no slumping).

The increase in mobility due to slumping is not expected to be significant at early times and it will predominately affect the top region of the reservoir, therefore equations (12) and (13) will only take effect after certain time (t_{slump}) and only for vertical positions $Z_D < Z_{slump}$, where Z_{slump} is a certain location that we specify. Otherwise, the original equations describing the model for the foam front displacement, (1) and (2), are used, supplemented by equations (8)–(9) in the event that concavities appear.

The increase in mobility will also affect the values of X_D and s_D at the top of the reservoir (for $Z_D = 0$). Therefore, from the boundary condition, equation (6), substituted into equations (1)–(3), these values are given by equation (14) for $t_D > t_{slump}$:

$$X_D(0,t) = s_D(0,t) = \sqrt{2M_{slump}\,(t_D - t_{slump}) + 2t_{slump} + s_{D0}^2}. \tag{14}$$

The program has been modified in order to incorporate this feature. The other modifications to the code to solve the system for slumping mainly affect the time derivatives of front positions, and intend to depict the slumping occurring after a certain time and the concave region developed as a consequence of this. It is

necessary to define some additional parameters such as the values of M_{slump}, t_{slump}, Z_{slump} in order to determine the modified front shape.

Specifically, the program has been modified via the construction of the conditional for the calculation of time derivatives ($\mathrm{d}X_D/\mathrm{d}t_D$, $\mathrm{d}Z_D/\mathrm{d}t_D$, etc.), and concavities are handled based on the sign of curvature and the magnitude of the turning angle θ: if $t_D < t_{slump}$, equations (1)–(2) are used for all the vertical points; if $t_D > t_{slump}$ and $Z_D < Z_{slump}$, equations (12) and (13) are applied; if $t_D > t_{slump}$ and $Z_D > Z_{slump}$, the code checks for negative values of curvature and the magnitude of the turning angle between intervals ($K < 0$ and $\theta > \theta_{sharp}$) and uses either equations (1)–(2) (for convex regions) or (8)–(9) if necessary (for concave regions).

Regarding the implementation of equation (14) for the top boundary, an 'if' construction has also been used. As mentioned previously, this equation is applied for $t_D > t_{slump}$. On the other hand when, $t_D < t_{slump}$, the right hand side of equation (14) is replaced by $\sqrt{2t_D + s_{D_0}^2}$, which again is compatible with equation (6).

The following section gives results for the numerical solution of the slumping case.

4. Results

This section presents the results of modelling slumping specifically in the case where the concavities that can develop as a consequence of it are propagated at a higher speed (as per equations (8)–(9)) than adjacent convex regions, in addition to slumped regions moving faster (as per equations (12)–(13)) than unslumped ones.

The front was discretised into 100 segments, with values of angle α determined for each segment. Time evolution was achieved via a Heun method: this is a predictor-corrector method where an estimate is made of the solution at the end of a time step, and then that estimate is revised based on rates of change averaged at the beginning and end of the step. We used a time step 1×10^{-5}. New segments were added to the discretised front, whenever segment length increased by a factor of 0.25. Likewise segments were removed whenever their length shrunk down to 0.002. The values of s_{D_0} and θ_{sharp} were 0.001 and $\pi/18$ as mentioned previously. In addition, the following parameters (chosen arbitrarily to illustrate the model for slumping) are used: $M_{slump} = 2.5$, $t_{slump} = 0.5$, and $Z_{slump} = 0.25$.

We emphasise that these slumping parameters are arbitrary choices to elucidate the typical behaviour of the model. There are modifications we could make to the slumping model which would arguably make it more realistic. For example the parameter Z_{slump} could be taken to be a function of time t_D, with Z_{slump} growing according to the value of $t_D - t_{slump}$. Likewise the parameter M_{slump} could be taken to be a function of $Z_{slump} - Z_D$: the value of M_{slump} growing with $Z_{slump} - Z_D$. In the present work however, we consider the simple model for which all our slumping parameters are treated as constants.

Figure 4 shows the plot obtained where a concave region tends to develop transiently on the front. However this concave region has a different form from what was postulated in Figure 3. Specifically it does not remain fixed at $Z_D = Z_{slump}$ but instead migrates downwards. Despite this downward migration, the concavity itself remains contained within a section of the front of rather limited extent. Eventually the concavity approaches the bottom of the front at $Z_D = 1$.

This concave region then has little long term impact on the overall front shape for at least two reasons. Firstly, when Z_D is close to 1 velocities of points on the

front are very small (note that velocities vanish identically when Z_D is exactly 1), so the front is barely advancing there. Secondly, when the concave region is close to the bottom of the front, the local front orientation is actually quite close to horizontal.

The significance of the local near horizontal orientation, is that concave points are higher up than convex ones. Concave points then have an 'extra' effect helping them to catch up with convex ones: not only do they benefit from the $\cos(\theta/2)$ factor in the denominator of equations (8)–(9), but also from the fact that $1 - Z_D$ for concave regions (albeit being much smaller than unity) is actually slightly larger than for convex ones.

At longer times the concavity has little impact on the front shape (as we have stated), and for the overwhelming majority of Z_D values, the front is convex. The really notable feature of the convex shape observed for later times however, is that it has a kink at position $Z_D = Z_{slump}$. In other words, quite differently from the speculations offered in [3] about possible concave kinks, we actually see a convex one.

This is suggestive of a long-time asymptotic state limit in which the entire front both above and below location Z_{slump} propagates with an *apparent* horizontal velocity which is uniform at all spatial locations. The corresponding analysis is presented in the next section.

5. Analytical solution for slumping

Here the analysis of the system of equations (12)–(13) for slumping and their matching onto equations (1)–(2) lower down that can be considered valid for long times is presented; this is the long-time asymptotic state (front shape) where the whole front propagates at the same apparent velocity.

5.1. Analytical solution in the slump zone

At a large time $t_D \gg 1$, the top of the foam front has displaced, according to equation (14):

$$X_D \approx s_D \approx \sqrt{2M_{slump}t_D} \tag{15}$$

where the value of s_{D0}^2 and t_{slump} in equation (14) are negligible for long times. The approximation we make at long times [3] is that all points on the front (except those at Z_D exceedingly close to unity) have displaced through nearly the same distance, as given by equation (15).

The long-time asymptotic solution for the slumping case follows:

$$\frac{\mathrm{d}X_D}{\mathrm{d}t_D} \approx \frac{M_{slump}\,(1 - Z_D)\cos\alpha}{\sqrt{2M_{slump}t_D}} \tag{16}$$

$$\frac{\mathrm{d}Z_D}{\mathrm{d}t_D} \approx \frac{M_{slump}\,(1 - Z_D)\sin\alpha}{\sqrt{2M_{slump}t_D}}. \tag{17}$$

Defining Y_D as $Y_D = 1 - Z_D$ and a complementary angle α_c to α, as shown in Figure 5, equations (16) and (17) are expressed as:

$$\frac{\mathrm{d}X_D}{\mathrm{d}t_D} \approx \frac{M_{slump}Y_D\sin\alpha_c}{\sqrt{2M_{slump}t_D}} \tag{18}$$

$$\frac{\mathrm{d}Y_D}{\mathrm{d}t_D} \approx -\frac{M_{slump} Y_D \cos\alpha_c}{\sqrt{2 M_{slump} t_D}}. \tag{19}$$

The similarity variable is defined as ξ_{slump} and measures the displacement between a point of the front and the leading edge at the top of the front:

$$\xi_{slump} = X_D - \sqrt{2 M_{slump} t_D}. \tag{20}$$

A solution for ξ_{slump} as a function of Y_D is required.

Following an analysis as in the case of a homogeneous system [3], the derivative $\mathrm{d}Y_D/\mathrm{d}\xi_{slump}$ is

$$\frac{\mathrm{d}Y_D}{\mathrm{d}\xi_{slump}} = \frac{Y_D \cos\alpha_c}{1 - Y_D \sin\alpha_c} \tag{21}$$

which is a similar expression as for the homogeneous case ($\mathrm{d}Y_D/\mathrm{d}\xi$), where ξ is the displacement between a point X_D and the leading edge of the front without slumping. Using equations (22) and (23) for $\cos\alpha_c$ and $\sin\alpha_c$,

$$\cos\alpha_c = \frac{1}{\sqrt{1 + (\mathrm{d}Y_D/\mathrm{d}\xi_{slump})^2}} \tag{22}$$

$$\sin\alpha_c = \frac{\mathrm{d}Y_D/\mathrm{d}\xi_{slump}}{\sqrt{1 + (\mathrm{d}Y_D/\mathrm{d}\xi_{slump})^2}} \tag{23}$$

equation (21) can be expressed as:

$$\frac{\mathrm{d}Y_D}{\mathrm{d}\xi_{slump}} = \frac{Y_D}{\sqrt{1 - Y_D^2}} \tag{24}$$

the integral of which is:

$$-\xi_{slump} = -\sqrt{1 - Y_D^2} + \log\frac{1}{Y_D} + \log\left(\sqrt{1 - Y_D^2} + 1\right). \tag{25}$$

The format of this equation emphasises that $\xi_{slump} < 0$ and $Y_D < 1$.

The equation for ξ_{slump} in terms of Z_D is:

$$\xi_{slump} = \sqrt{1 - (1 - Z_D)^2} + \log(1 - Z_D) - \log\left(\sqrt{1 - (1 - Z_D)^2} + 1\right). \tag{26}$$

Therefore, the similarity variable in terms of Z_D (or Y_D) is the same as in the case for a homogeneous system. What is different here, from the previous case, is the definition of ξ_{slump}, in terms of X_D and t_D and M_{slump}, given by equation (20).

The front shape obtained with the asymptotic solution, given the interval for values of the coordinate Z_D and the final time required t_D is calculated using equations (26) and (20). Figure 6 depicts analytical results, for both cases with slumping and without slumping, for $t_D = 50$ (with $M_{slump} = 2.5$ for slumping).

The asymptotic solution has the same shape for the case of a homogeneous system, the difference in this case is the definition of ξ_{slump} which is affected by the increase in mobility, thereby making the displacement of the front greater for the slumping case, i.e. the X_D values are larger.

Figure 7 compares the asymptotic solution to the numerical solution. The analytical calculations use $M_{slump} = 2.5$; regarding the numerical results, the program

is used with $M_{slump} = 2.5$, as well as $t_{slump} = 0.5$, and $Z_{slump} = 0.25$. Both cases are for $t_D = 50$.

The numerical data seem to match the analytical solution in the region affected by the increase in mobility ($0 < Z_D < Z_{slump}$) but has a sharp turn away from the analytical solution immediately below this region. However, the curves do not exactly match even in the region $0 < Z_D < Z_{slump}$, as can be seen in the inset in Figure 7 (at least for $t_D = 50$); this is because the terms containing t_{slump} are not taken into account in the calculation of the analytical solution leading to a displacement that is slightly faster for this case. This mismatch is however really very small (and arises due to our approximation that all points on the front have displaced by the same uniform amount $\sqrt{2M_{slump}t_D}$).

The feature of the sharp turn in the numerical solution is important. The sharp turn reflects a jump in the mobility occurring at Z_{slump}. The change in mobility requires a change in the tangent angle (α) to maintain the apparent horizontal propagation velocity of the front as a whole. It is this property of the solution, which we can use to derive a new analytical solution in the domain $Z_D > Z_{slump}$, that then agrees well with the numerical data.

5.2. Analytical solution in the zone that is not slumped

The condition that the front propagates at a uniform apparent horizontal velocity implies that

$$\frac{u_{perp}}{\cos\alpha} = \frac{\mathrm{d}s_{D,top}}{\mathrm{d}t} \tag{27}$$

where u_{perp} is the perpendicular front speed and the right hand side of equation (27) is the speed of the leading edge at the top of the reservoir which follows from equation (14). Note that equation (27) applies both inside and outside the slump zone.

In the slump zone (in terms of Y_D)

$$u_{perp} = \frac{Y_D M_{slump}}{s_{D,top}}. \tag{28}$$

Substituting the expression from equation (27) into (28) and using (15) for the value of $s_{D,top}$, we can deduce

$$Y_D = \cos\alpha \tag{29}$$

which in terms of α_c is

$$Y_D = \sin\alpha_c. \tag{30}$$

Recall that, $u_{perp}/\sin\alpha_c$ must be continuous at $Z_D = Z_{slump}$; however for the slumping case u_{perp} falls by a factor $1/M_{slump}$ at that point and also $\sin\alpha_c$ must fall by the same factor.

In fact for $Z_D > Z_{slump}$, we obtain

$$\sin\alpha_c = \frac{Y_D}{M_{slump}}. \tag{31}$$

Substituting the value of $\sin\alpha_c$ from equation (23) into (31) and rearranging, a

formula for $\mathrm{d}\xi_{slump}/\mathrm{d}Y$ is obtained (now valid for $Z_D > Z_{slump}$):

$$\frac{\mathrm{d}\xi_{slump}}{\mathrm{d}Y_D} = \sqrt{\frac{M_{slump}^2}{Y_D^2} - 1} \tag{32}$$

the solution of which is

$$\begin{aligned} -\xi_{slump} = -\xi_{match} - M_{slump}\sqrt{1 - \frac{Y_D^2}{M_{slump}^2}} + M_{slump}\log\left(\frac{M_{slump}}{Y_D}\right) + \\ M_{slump}\log\left(\sqrt{1 - \frac{Y_D^2}{M_{slump}^2}} + 1\right) + M_{slump}\sqrt{1 - \frac{Y_{match}^2}{M_{slump}^2}} - M_{slump}\log\left(\frac{M_{slump}}{Y_{match}}\right) - \\ M_{slump}\log\left(\sqrt{1 - \frac{Y_{match}^2}{M_{slump}^2}} + 1\right) \end{aligned} \tag{33}$$

where ξ_{match} is obtained through equation (26) with $Z_D = Z_{slump}$.

Figure 8 presents the comparison between the numerical results, obtained for $t_D = 50$ with $M_{slump} = 2.5$, $t_{slump} = 0.5$ and $Z_{slump} = 0.25$; and the curve obtained from the combination of equations (26) and (33) for the analytical solution for $M_{slump} = 2.5$ and $Z_{slump} = 0.25$.

Now with the correct equation to describe the interval $Z_D > Z_{slump}$, the analytical results follow the shape of numerical data very closely. At $Z_D = Z_{slump}$ the analytical curve also presents the expected sharp turn. Note also that for small X_D values the analytical predictions are at smaller Z_D values, i.e. higher Y_D values than the numerical ones: this is a manifestation of the numerical solution approaching $Z_D = 1$ at $X_D = 0$, but the analytical solution only doing so asymptotically as $X_D \to -\infty$. Despite the small discrepancy with the asymptotic results for Z_D near unity, the numerical solutions make it clear that we are dealing with a segment of front that is both very near horizontal at $Z_D = 1$ and very near stationary.

Considering Z_D values higher up, note also that even points located in the region which is not slumped have displaced further than would be the case with no slumping whatsoever (see Figure 6). This is because points in the region which is not slumped historically have spent part of their evolution in the slump zone, where they were more mobile. In the model as formulated, material points lose mobility immediately once they leave the slump zone. Had we formulated the model in such a way that material points, once they entered a slump zone, retained high mobilities for all times thereafter, the advance of the front would be greater still (more akin to the analytic curve in Figure 7).

Observe that compared to the unslumped case, the results for slumping in Figure 8 indicate that the front is less uniform with depth, i.e. a greater area of the reservoir underneath the foam front (measured back from the leading edge at the top) remains unswept. Nevertheless the reservoir sweep indicated by equation (33) is still relatively efficient: equation (33) indicates a Y_D value decaying towards zero over a characteristic horizontal distance M_{slump} back from the leading edge of the front, which is much less than the distance $\sqrt{2M_{slump}t_D}$ that the leading edge itself advances for large t_D.

The last section offers conclusions about the results presented so far.

6. Conclusions

We have presented numerical and analytical results for an idealized model of foam front propagation in an oil reservoir in the case of slumping. Specifically slumping (of surfactant) is assumed to enhance coarsening and collapse of bubbles near the top of the reservoir which will cause an increase in mobility in that zone.

This process is described by a model based on the case presented by Shan and Rossen [1] (the pressure-driven growth model), taking into account the feature of change in mobility. First of all, numerical data were obtained with the modified equations describing the foam front advance. From these results, an interesting behaviour was observed (specifically a convex kink at the height to which surfactant slumps), leading to the long-time asymptotic analysis of this case from which two expressions have been obtained and matched at the kink to describe surfactant slumping analytically.

Our results have addressed just one out of several open research questions that arise with the pressure-driven growth model: other open questions (that have already been identified by [3]) include what happens if there is an increase in the injection pressure during the course of the injection process, and moreover what happens if the reservoir itself is heterogeneous. As we mentioned in the introduction, such cases will be addressed in future work.

It is worth remembering also that pressure-driven growth is itself an idealized model, in the sense that it assigns finite mobilities only to the foam front, with mobilities assumed to be infinite everywhere else. We have managed to model surfactant slumping using pressure-driven growth, but liquid slumping (a related phenomenon, which tends to occur quite some distance behind the foam front, rather than at the foam front itself) needs more sophisticated models, which must be able to consider variation of mobilities throughout the whole reservoir.

Acknowledgements

EMH acknowledges scholarship funding from EPS-CONACyT programme. PG acknowledges sabbatical stay funding CONICET Argentina res. no. 2218/13.

Appendix A. Background to the pressure-driven growth model

Here we give the background to the pressure-driven growth model. Full details can be found in the original references [1, 2, 3].

The discussion is laid out as follows. Section Appendix A.1 describes the assumptions underlying the model. Next section Appendix A.2 gives the governing equations in dimensional form (those in the main text having been given in dimensionless form). Singularities in and stability of the solutions are considered in sections Appendix A.3–Appendix A.4 respectively.

Appendix A.1. Assumptions underlying the pressure-driven growth model

We consider the surfactant alternating gas process in which an oil reservoir is flooded first with liquid surfactant solution and then gas is injected to form foam in situ. A foam front develops at the boundary between the liquid and gas, and migrates forward displacing the liquid with the ultimate aim of increasing the amount of oil that is recovered. Thus ahead of the moving foam front we have a liquid bank whereas behind the foam front we have a gas bank (or more precisely a foam bank).

There are advantages [1] to using foam to displace oil from a reservoir compared to other recovery strategies (e.g. injecting gas alone without surfactant and hence without foam). Whereas gas alone, which has comparatively low viscosity, tends to be subject to fingering instabilities (i.e. it finds preferential flow paths through the reservoir leaving significant amounts of liquid in place) this tends not to happen with foam. The reason fingering is suppressed is because the presence of foam films greatly augments the resistance to gas flow through the porous medium of the reservoir. Films can for instance block off certain pores to gas flow. Moreover if gas manages to flow along a pore spanned by a film, then the film must move also, and such film motion is surprisingly dissipative [13, 14].

The foam improved oil recovery process involves multiphase flow in a porous medium, which is more complicated than single phase flow [15]. Conventionally a single phase flowing in a porous medium is described via Darcy's law, such that fluid fluxes are proportional to the driving pressure gradient, proportional to the medium permeability and proportional to the mobility of the fluid (the reciprocal of its viscosity). The interstitial velocity of fluid through the medium can be deduced given the flux, assuming the medium porosity is known. In the case of multiphase flow, the motion of the different phases (e.g. liquid and gas) can be described once again by Darcy's law but with correction factors (relative permeabilities or relative mobilities) representing the fact that for a given pressure gradient the flux of any given phase is less in a multiphase system than in a single phase one. Again interstitial velocities of phases can be obtained from the fluxes, given the medium porosity and given the fraction of the pore space filled by each phase.

In the case of interest here, we have a very particular multiphase system with a foam bank and a liquid bank separated by a foam front. The presence of foam reduces the relative mobility of gas both in the foam bank and at the foam front, without of course affecting the liquid bank [1]. However the relative mobility for gas at the foam front is much lower than further back in the foam bank [1]. The reason is that further back the foam is drier, and since the films tend to collapse as the foam dries out, the number density of foam films is highest at the front, but substantially lower further back in the foam bank. Since it is the foam films that restrict gas motion, the relative mobility at the front is far lower than anywhere else in the system.

Accordingly Shan and Rossen [1] supposed that the entire pressure drop driving the flow occurred just across the foam front, instead of pressure drops being distributed over the entire medium. This driving pressure drop is the difference between the injection pressure of the gas, and the hydrostatic pressure in the reservoir (the latter dependent on depth). The top of the foam front advances faster than the rest of the front as there is no opposing hydrostatic pressure at the top. Sufficiently deep down in the reservoir the gas cannot advance at all, because a point is reached where the hydrostatic pressure exactly balances the injection pressure.

In the above discussion we have not said anything about the structure of the foam front merely treating it as the interface between the foam bank and the liquid bank. In reality the foam front (itself containing a very large number of bubbles and films) has a finite thickness (up to the order of hundreds of metres whilst the liquid bank and foam banks and the reservoir itself extend much further, especially in the horizontal direction, for several kilometres [3]). The pressure gradient within the front is then finite, being the aforementioned pressure drop divided by the front thickness, with the direction of the pressure gradient vector (and hence the direction

of the flow it induces) being normal to the front.

The front thickness is not constant over time. Fractional flow theory (see [1, 16, 17]) indicates that the forward boundary of the foam front moves at slightly higher speed than the rear boundary. This means that the foam front spreads by an amount proportional to the distance it has propagated (albeit the coefficient of proportionality is typically much smaller than unity). The proportionality coefficient depends on exactly where the low mobility foam front is considered to join onto the comparatively higher mobility foam bank. This is sensitive to the assumed bursting/collapse process of the foam as it dries out.

Appendix A.2. Governing equations in dimensional form

Taking into account the discussion above, governing equations for pressure-driven growth can be obtained, which are dimensional analogues of equations (1)–(2) are

$$\frac{\mathrm{d}X}{\mathrm{d}t} = \frac{k\lambda_r}{(1-S_w)\phi}\frac{\rho g(Z_{max}-Z)\cos\alpha}{\tau s} \tag{A.1}$$

$$\frac{\mathrm{d}Z}{\mathrm{d}t} = \frac{k\lambda_r}{(1-S_w)\phi}\frac{\rho g(Z_{max}-Z)\sin\alpha}{\tau s} \tag{A.2}$$

where X is dimensional horizontal coordinate, Z is dimensional vertical coordinate (measured downwards), s is dimensional distance that the front has travelled, and t is dimensional time. Meanwhile k is the reservoir permeability, λ_r is the gas relative mobility at the foam front (relative mobility being the reciprocal of an effective viscosity), S_w is the volume fraction of liquid in the foam, ϕ is the porosity of the reservoir, ρ is the density difference between the aqueous liquid region (ahead of the foam) and the gas within the foam, and g is gravity. Moreover Z_{max} is the maximum depth to which foam can penetrate, which for a pressure P_{drive} driving the injection, is determined by $Z_{max} = P_{drive}/(\rho g)$. Additionally τ is the proportionality ratio between the thickness of the wet foam region and the distance that the front has travelled, which by assumption is a small parameter.

Distances are made dimensionless on the scale Z_{max} whilst times are made dimensionless on the scale

$$t_{scale} = \frac{(1-S_w)\phi}{k\lambda_r}\frac{Z_{max}^2}{P_{drive}}\tau. \tag{A.3}$$

We can give an estimate of these scales as follows. With a driving pressure P_{drive} of 2.4×10^6 Pa given by [1], a density difference ρ of order 1000 kg m^{-3}, and gravity g of 9.8 m s^{-2}, we obtain $Z_{max} = 265$ m. Later work by [2] obtained $Z_{max} = 2200$ m but for a substantially bigger driving pressure. We are interested moreover in horizontal distance scales rather larger than these vertical ones.

Meanwhile for a permeability of k of 2.95×10^{-13} m^2, and a relative mobility of 243 Pa^{-1} s^{-1} (both values given by [1]), assuming a low liquid fraction S_w in the foam rather less than unity, adopting the value $Z_{max} = 265$ m given here, and estimating $\tau = 0.01$ as in [3], we can compute t_{scale} as being on the order of 11 days.

Appendix A.3. Singularities in solutions of the pressure-driven growth model

Although the governing equations (A.1)–(A.2) appear comparatively simple, they have been shown to be very challenging to solve numerically with certain numerical schemes proving susceptible to instabilities [2, 3]. The underlying reasons for this

have been studied by [3] who showed that the solutions of the equations themselves admit singularities. The most severe type of singularity was found to occur when a front contained a concavity (as seen from the liquid bank). The concavity evolved over time in such a way as to focus down to a point. Once that happened, two otherwise convex sections of front would meet at concave corner. This represented a singularity because the tangent to the front underwent a jump (i.e. a change in direction) at the corner.

The situations of main interest studied by [3] actually involved convex shapes, rather than concave ones, making these 'sharp corner' singularities less prevalent. Those solutions still exhibited other types of singularities however, in particular at the top boundary of the foam front. Specifically if one moved a small (dimensionless) depth Z_D vertically into the reservoir, the horizontal location of the front moved a distance on the order of $Z_D^{3/2}$ behind the horizontal location of the leading edge at the top of the front. The implication is that the curvature at the top of the front diverges near the top like $Z_D^{-1/2}$.

The detailed mathematical derivation of this singularity is given in [3], but the physical reason it appears can be explained as follows.

The top of the front must be vertical to ensure that the motion there is parallel to the top boundary of the reservoir. The curvature near the top of the front defines on purely geometric grounds, the horizontal displacement between a point slightly below the top of the front and the leading edge at the top.

There is however a second way to compute this horizontal displacement which needs to be compatible with the first. Material points near the top of the front move primarily horizontally, but also have slight tendency to migrate downwards. The more sharply the front curves near the top, i.e. the more quickly the normal to the front acquires a significant component along the vertical, the more rapid this downwards migration becomes. The horizontal velocity component of front material points falls as these points migrate downwards, primarily because the pressures driving these points are opposed by higher hydrostatic pressures. The horizontal displacement between a material point slightly below the top of the front and the leading edge at the top is then given by the deficit in horizontal velocity component integrated over the time that is required to migrate to a given depth.

Consider for example a hypothetical case for which the front is assumed to curve only extremely weakly near the top and thus is almost perfectly vertical. On geometric grounds, front points near the top then are displaced horizontally hardly at all with respect to the leading edge at the top. However front points also have exceedingly slow downward migration (as the vertical component of the front normal is extremely small). This however leads to a contradiction: front points below the top have taken an arbitrarily long time to migrate downwards to their current location and so, during this migration, should have fallen an arbitrarily long distance behind the leading edge. This is incompatible with the edge being almost perfectly vertical.

In fact the same argument applies for any finite curvature at the top. As long as curvature is finite, points arbitrarily close to the top can be made to start their vertical migration arbitrarily slowly. Hence points at given distance below the top still take an arbitrarily long time to migrate to their current location and so should have fallen an arbitrarily long distance behind the leading edge. This is incompatible with a finite curvature.

By introducing a weak singularity in curvature at the top boundary such that the horizontal displacement of the front relative to the leading edge grows like the $\frac{3}{2}$

power of depth, we ensure that material points released exactly at the top boundary can migrate a finite distance vertically away from the top boundary during a finite time. During this finite time, the cumulative amount that they fall behind the leading edge (owing to the deficit in their horizontal velocity component) exactly matches the assumed curve shape.

The fact that the singularity in curvature allows a point released from the top boundary to migrate vertically away from the top boundary comparatively rapidly (compared to a case with finite curvature) has implications for a numerical scheme [3]. It becomes necessary to subdivide the topmost numerical interval very often, and the way that subdivision is done should reflect the known singular variation of X_D with Z_D that applies there.

The above analysis applies to the case of a front which is infinitesimally thin. In case of a front of small but finite thickness the curvature singularity is relaxed: the front cannot curve more sharply than its finite thickness permits. Despite the finite curvature, the paradox of points at depth appearing to fall arbitrarily far behind the leading edge no longer arises: the velocity of the top of a finite thickness front becomes weakly sensitive to the curvature suppressing the otherwise problematic velocity deficit [3].

Appendix A.4. Stability of solutions of the pressure-driven growth model

The reason why the pressure-driven growth model is challenging to solve numerically, and likewise the reason why it admits the singular solutions referred to above, is that the model itself is 'neutrally stable', right on the borderline of turning unstable. The model per se does not assign any 'energy cost' to either sharp corners or diverging curvatures on fronts, which is why these are admitted within solutions.

Grassia et al. [3] have discussed stability of the model at length. The governing equations here are hyperbolic partial differential equations [18]. They are advection equations, such that disturbances to the front shapes tend in the first instance to be advected along, instead of either growing or decaying exponentially.

It is possible to stabilize the equations by adding a weak diffusive term, and Grassia et al. [3] did this. The resulting equations are then advection-diffusion equations: these are of parabolic type [18]. The diffusive term even has a physical interpretation [3]: the foam front is an object of small but finite thickness, and the diffusive term prevents it from being bent into a radius of curvature smaller than its thickness. What the diffusion term does is relax the concave corners produced by the original 'non-diffusive' advection equation replacing them by concave regions of large but finite curvature. It also relaxes the convex singularity (where curvature diverges) on the top boundary, again making it into a region of large but finite curvature. These are effectively 'curvature boundary layers' (a concept discussed by [19]) and they match onto regions of much lower curvature where diffusive terms are not required.

The parabolic advection-diffusion equations whilst definitely stable are stiff numerically [3]. One must resolve the dynamics on the fine scale of the curvature boundary layers, even though the results of interest are on the much larger scale of the entire reservoir. Grassia et al. [3] therefore explored solution methods for the original advection equations, extracting the foam front shapes of interest outside the curvature boundary layers, and keeping the curvature boundary layers contained or localised at isolated points without needing to resolve their structure.

As we are now back to dealing with hyperbolic partial differential equations, the solutions exhibit the mathematical features known to occur for that class of equations, namely characteristics (front material points correspond to characteristics), discontinuous shocks (concave corners are shocks) and fans (the convex curvature singularity at the top of the foam front is a fan) [3]. An important contribution of Grassia et al. [3] was to determine how to propagate the shocks (i.e. concavities), which turn out to have higher velocity than the characteristics (front material points). The sharper the corner, the faster it must propagate.

The equations are neutrally stable in the sense that a small disturbance to the shape of the foam front exhibits neither exponential growth nor exponential decay. This does not imply that such disturbances do not evolve at all: in fact disturbances are advected along fronts and evolve as the front geometry evolves [3]. Disturbances in the fan region can spread along the front as the fan itself spreads out. Disturbances can also evolve into concave shocks themselves. Information is lost at the concave shocks since material points are consumed there. A disturbance located close by to a shock might well be consumed by a shock and thereby cease to exist.

The overall tendency however is for both material points and shocks to migrate over time to the bottom of the solution domain. Driving pressures are balanced by hydrostatic pressures at the bottom of the domain so that the front is horizontal and stationary there. All disturbances to the front eventually reach this 'dead zone' and do not impact thereafter on the front shape.

References

[1] D. Shan, W. R. Rossen, Optimal Injection Strategies for Foam IOR, SPE J. 9 (2) (2004) 132–150.

[2] R. M. de Velde Harsenhorst, A. S. Dharma, A. Andrianov, W. R. Rossen, Extension and verification of a simple model for vertical sweep in foam SAG displacements, SPE Reservoir Evaluation & Engg 17 (2014) 373–383.

[3] P. Grassia, E. Mas-Hernández, N. Shokri, S. J. Cox, G. Mishuris, W. R. Rossen, Analysis of a model for foam improved oil recovery, J. Fluid Mech. 751 (2014) 346–405.

[4] L. L. Schramm, F. Wassmuth, Foams: Basic principles, in: L. L. Schramm (Ed.), Foams: Fundamentals and Applications in the Petroleum Industry, no. 242 in Advances in Chemistry, American Chemical Society, Washington, DC, 1994, Ch. 1, pp. 3–45.

[5] J. J. Bikerman, Foams: Theory and Industrial Applications, Reinhold Publishing Corporation, New York, 1953.

[6] D. L. Weaire, S. Hutzler, The Physics of Foams, Clarendon Press, 1999.

[7] P. Grassia, S. J. Neethling, C. Cervantes, H. T. Lee, The growth, drainage and bursting of foams, Colloids and Surf. A: Physicochem. and Engg Aspects 274 (1–3) (2006) 110–124.

[8] S. Hutzler, D. Weaire, S. Shah, Bubble sorting in a foam under forced drainage, Phil. Mag. Lett. 80 (1) (2000) 41–48.

[9] S. Hutzler, D. Weaire, Foam coarsening under forced drainage, Phil. Mag. Lett. 80 (6) (2000) 419–425.

[10] M. Tong, K. Cole, S. J. Neethling, Drainage and stability of 2D foams: Foam behaviour in vertical Hele-Shaw cells, Colloids and Surf. A: Physicochem. and Engg Aspects 382 (1–3) (2011) 42–49.

[11] G. J. Hirasaki, The steam-foam process, J. Pet. Technol. 41 (5) (1989) 449–456.

[12] A. R. Kovscek, H. J. Bertin, Foam mobility in heterogeneous porous media, Transport in Porous Media 52 (1) (2003) 17–35.

[13] I. Cantat, N. Kern, R. Delannay, Dissipation in foam flowing through narrow channels, Europhys. Lett. 65 (2004) 726–732.

[14] S. A. Jones, B. Dollet, Y. Méheust, S. J. Cox, I. Cantat, Structure-dependent mobility of a dry aqueous foam flowing along two parallel channels, Phys. Fluids 25 (2013) 063101.

[15] M. Sahimi, Flow and Transport in Porous Media and Fractured Rock: From Classical Methods to Modern Approaches, 2nd Edition, Wiley-VCH Publishers, Weinheim, Germany, 2011.

[16] Z. H. Zhou, W. R. Rossen, Applying fractional-flow theory to foam processes at the 'limiting capillary pressure', SPE Advanced Technology Series 3 (1995) 154–162.

[17] W. R. Rossen, S. C. Zellinger, J.-X. Shi, M. T. Lim, Simplified mechanistic simulation of foam processes in porous media, SPE J. 4 (1999) 279–287.

[18] M. Renardy, R. C. Rogers, An Introduction to Partial Differential Equations, 2nd Edition, Vol. 13 of Texts in Applied Mathematics, Springer-Verlag, New York, Berlin, Heidelberg, 2004.

[19] P. Grassia, G. Montes-Atenas, L. Lue, T. E. Green, A foam film propagating in a confined geometry: Analysis via the viscous froth model, Eur. Phys. J. E 25 (2008) 39–49.

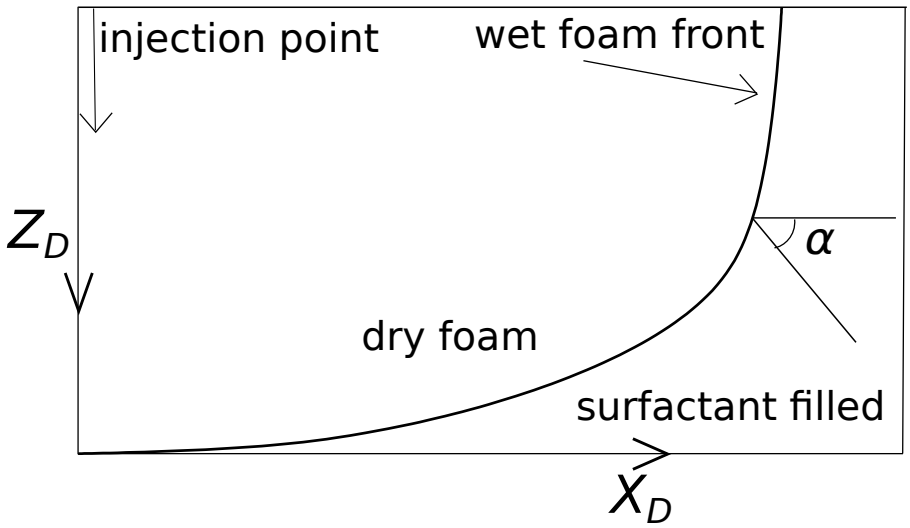

Figure 1: Schematic of a foam front displacement. The region to the right of the front is filled with liquid (surfactant solution): this is the so called 'liquid bank'. The region to the left of the front up to the gas injection point is filled with dry foam with comparatively large bubbles: this is the so called 'gas bank' or 'foam bank'. The wet foam region at the front itself (where bubbles are comparatively small) that provides the dominant resistance to motion. The horizontal coordinate X_D and vertical coordinate Z_D (measured downwards) and the angle α are indicated on the figure.

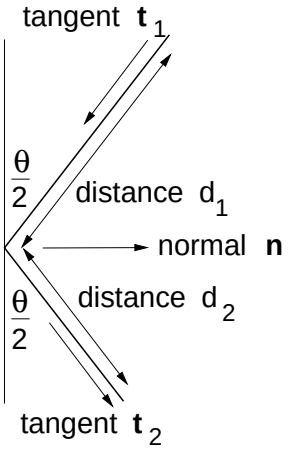

Figure 2: Two discrete elements of front turning through an angle θ. Tangent vectors as $\mathbf{t_1}$ and $\mathbf{t_2}$, element lengths are d_1 and d_2 and the normal vector is $\mathbf{n}$.

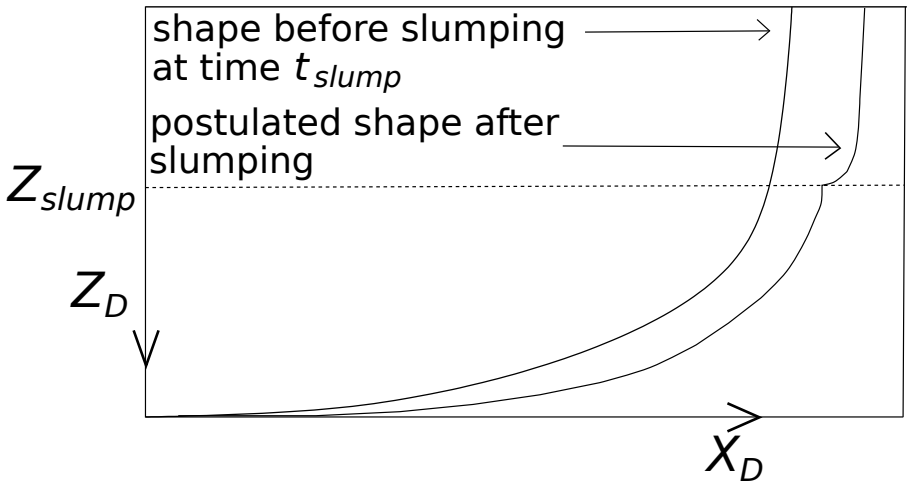

Figure 3: Schematic of the slumping case as postulated by [3]. Front propagates as normal until a certain time, after which the mobility of the upper part of the front (i.e. the region higher up than Z_{slump}) is increased, causing it to run ahead of parts of the front lower down. The postulate was that a concavity might develop [3] at Z_{slump} as shown, and we intend either to prove or disprove that postulate.

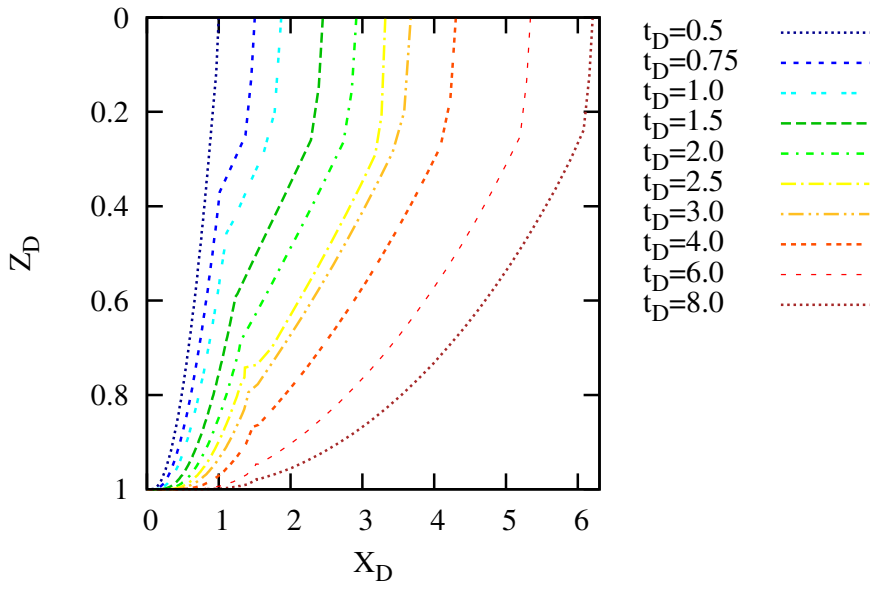

Figure 4: Foam front displacement at various times t_D for the slumping case. The parameters used (which have been chosen arbitrarily to illustrate the model) are $M_{slump} = 2.5$, $t_{slump} = 0.5$, and $Z_{slump} = 0.25$.

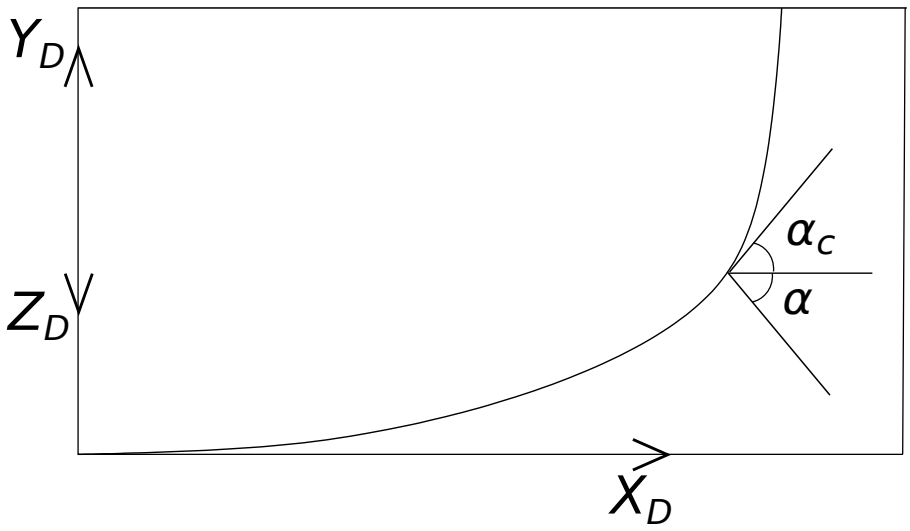

Figure 5: Schematic front displacement showing (in addition to coordinates X_D and Z_D and angle α), the direction of Y_D and the angle α_c.

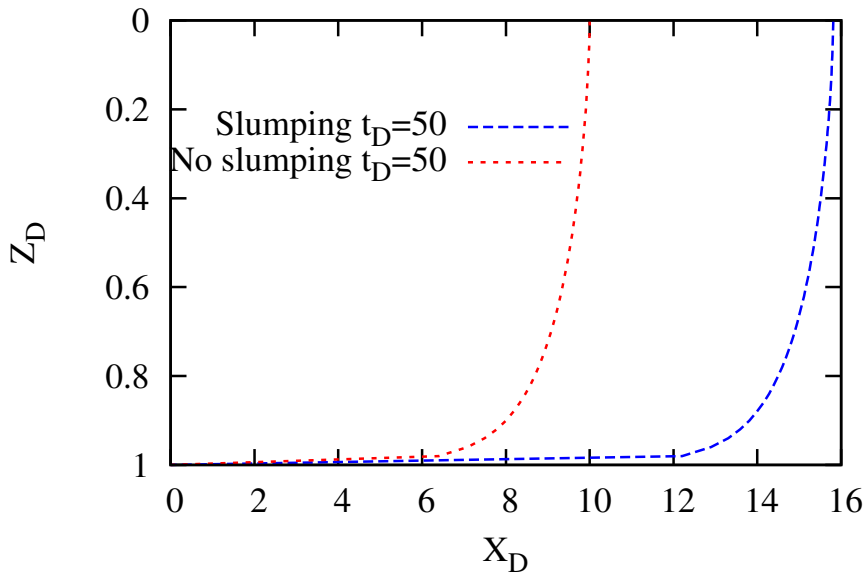

Figure 6: Asymptotic foam front at $t_D = 50$. For the slumping case $M_{slump} = 2.5$. Strictly speaking this solution should only apply for $Z_D < Z_{slump}$, with $Z_{slump} = 0.25$ here. For $Z_D > Z_{slump}$ it needs to be matched to another solution that preserves the apparent horizontal velocity across the point $Z_D = Z_{slump}$. For the case without slumping the solution is valid for all Z_D values.

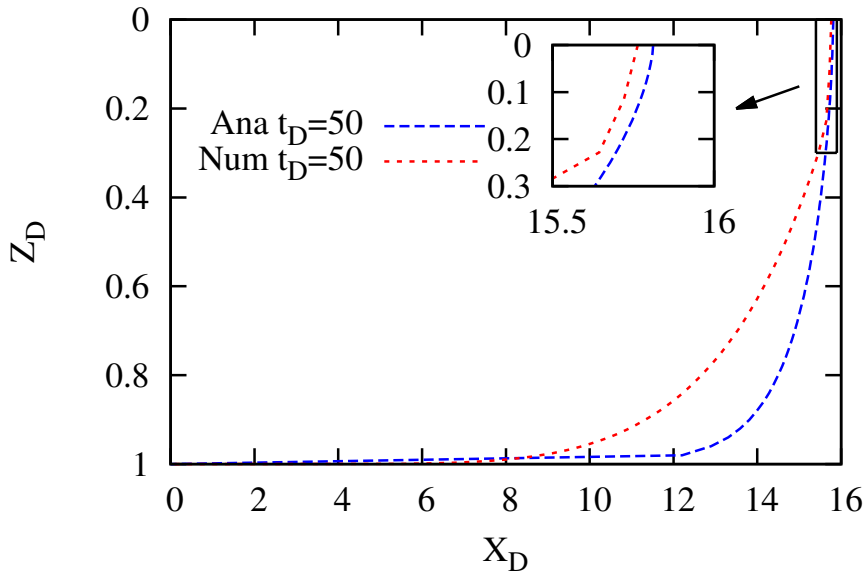

Figure 7: Foam front for slumping comparing the analytical results (Ana) to numerical (Num) at $t_D = 50$. The parameter used is $M_{slump} = 2.5$ in the analytical calculations, the numerical solution uses $M_{slump} = 2.5$, $t_{slump} = 0.5$, and $Z_{slump} = 0.25$.

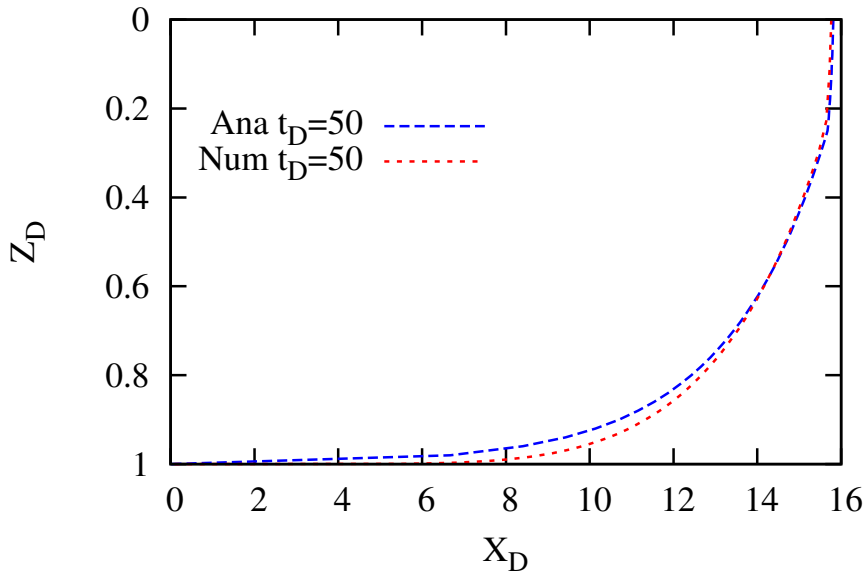

Figure 8: Comparison between analytical solution (Ana) obtained from the combination of equations (26) and (33) for $t_D = 50$ using $M_{slump} = 2.5$ and $Z_{slump} = 0.25$, and numerical results (Num) with $M_{slump} = 2.5$, $t_{slump} = 0.5$ and $Z_{slump} = 0.25$.